PCCP

PAPER

View Article Online
View Journal | View Issue

Cite this: *Phys. Chem. Chem. Phys.*, 2018, **20**, 30021

Influence of humidity and iron(III) on photodegradation of atmospheric secondary organic aerosol particles†

Pablo Corral Arroyo, [ab] Kurtis T. Malecha, [c] Markus Ammann [a] and Sergey A. Nizkorodov *[c]

Received 22nd June 2018,
Accepted 19th November 2018

DOI: 10.1039/c8cp03981j

rsc.li/pccp

The absorption of solar actinic radiation by atmospheric secondary organic aerosol (SOA) particles drives condensed-phase photochemical processes, which lead to particle mass loss by the production of CO, CO_2, hydrocarbons, and various oxygenated volatile organic compounds (OVOCs). We examined the influence of relative humidity (RH) and Fe(III) content on the OVOC release and subsequent mass loss from secondary organic aerosol material (SOM) during UV irradiation. The samples were generated in a flow tube reactor from the oxidation of D-limonene by ozone. The SOM was collected with a Micro Orifice Uniform Deposit Impactor (MOUDI) on CaF_2 windows. To selected samples, a variable amount of $FeCl_3$ was added before irradiation. The resulting SOM samples, with or without added $FeCl_3$, were irradiated with a 305 nm light-emitting diode and the release of several OVOCs, including acetic acid, acetone, formic acid and acetaldehyde, was measured with a Proton Transfer Reaction Time-of-Flight Mass Spectrometer (PTR-ToF-MS). The release of OVOCs from photodegradation of SOM at typical ambient mid-values of RH (30–70%) was 2–4 times higher than under dry conditions. The release of OVOCs was slightly enhanced in the presence of low concentrations of iron (0.04 Fe molar ratio) but it was suppressed at higher concentrations (0.50 Fe molar ratio) of iron indicating the existence of a complicated radical chemistry driving the photodegradation of SOM. Our findings suggest that the presence of iron in atmospheric aerosol particles will either increase or decrease release of OVOCs due to the photodegradation of SOM depending on whether the relative iron concentration is low or high, respectively. At atmospherically relevant RH conditions, the expected fractional mass loss induced by these photochemical processes from limonene SOA particles would be between 2 and 4% of particle mass per hour. Therefore, photodegradation is an important aging mechanism for this type of SOA.

Introduction

Organic compounds constitute a substantial fraction of atmospheric aerosol particles. They are present at an overall mass concentration that is comparable to that of major inorganic species such as sulfates, nitrates, sea salt and mineral dust components.[1] These organic compounds come from primary organic aerosol (POA), which is emitted directly by various sources, or from secondary organic aerosol (SOA), which is derived from reactions of volatile organic compounds (VOCs) with oxidants.[1] The distinction between the primary and secondary particles blurs as particles are aged by physical changes, such as gas-particle partitioning, particle coagulation or phase transitions within particles, and chemical processes such as reactive uptake of gas-phase oxidants by the particles.[2] Recent studies have shown that multiphase chemistry and photochemistry may significantly contribute to aging and particle growth.[2–4]

Particle phase photochemistry contributes to aerosol aging by multiple mechanisms. Energy-transfer or charge-transfer reactions driven by triplet states of organic compounds,[5–7] photolysis of nitrate and nitrite resulting in free radicals,[8] photochemistry of iron carboxylate or free iron,[9] and photolysis of carbonyls[10,11] are some of the examples of these processes. The condensed-phase photochemical reactions may not only change the SOA composition, but also change the volatility distribution of the SOA compounds resulting from photo-induced

[a] *Paul Scherrer Institute, Laboratory of Environmental Chemistry, 5232 Villigen PSI, Switzerland*
[b] *Department of Chemistry and Biochemistry, University of Bern, 2012 Bern, Switzerland*
[c] *Department of Chemistry, University of California, Irvine, California 92697, USA. E-mail: nizkorod@uci.edu; Fax: +1-949-824-8671; Tel: +1-949-824-1262*

† Electronic supplementary information (ESI) available: It describes the procedure for accounting for RH dependence of the PTR-ToF-MS ionization efficiency, and the kinetic multi-layer modelling of OVOCs diffusing through the photolyzed SOM sample. See DOI: 10.1039/c8cp03981j

fragmentation or oligomerization of SOA compounds into more or less volatile products.[12,13] The direct photolysis of organic compounds[14] or the secondary oxidation by HO_x radicals (HO_2 and OH) deriving from photolysis[15] explain the mass loss or decrease in particle size as well as the VOCs release observed in several studies related to photochemical processing of SOA.[16–19] For example, in our previous work we have shown that secondary organic material (SOM) is efficiently degraded by exposure to UV radiation producing CO, CO_2, small hydrocarbons,[11] as well as various oxygenated VOCs (OVOCs)[16,20,21] (in this paper, we are using "SOA" to refer to airborne particles, and "SOM" to the material formed by collecting bulk quantities of SOA particles on a substrate).

Relative humidity (RH) is an important environmental variable that affects not only physical properties but also chemistry occurring inside the particles. It has been well established that SOA particle viscosity depends strongly on RH.[22–24] Related to that, RH has a strong influence on diffusion-limited processes in SOA particles such as uptake or evaporation of chemical compounds or chemical reactions. For example, Ye and coworkers found that SOA particles from toluene oxidation resist exchange of semivolatile compounds at low relative humidity, but lose that resistance above 20% RH.[25] Shiraiwa *et al.* showed that the uptake coefficient of ozone to protein films varies with relative humidity due to the increase of the ozone diffusion coefficient with RH.[26] Similarly, Steimer *et al.* (2016) demonstrated a strong relationship between the steady state reactivity of ozone with shikimic acid and the estimated diffusivity of ozone as a function of relative humidity. Slade and Knopf showed that increasing RH enhances the OH uptake in levoglucosan particles due to the faster diffusion.[27] RH is also a key parameter controlling the rate of evaporation of OVOCs from SOA particles as shown by Yli-Juuti *et al.*[28] The RH was found to influence the photodegradation of 2,4-dinitrophenol through its effect on viscosity in several types of SOM including that generated by oxidation of D-limonene by ozone.[29,30] They observed a faster photodegradation at high RH due to the increase of the efficiency in the second-order degradation reactions, which are likely to be affected by the diffusion limitations of the excited state, and therefore, by the viscosity.[29] Atmospheric models are starting to take the RH-dependent viscosity into consideration and confirm that aerosol particles can be liquid, semisolid or solid depending on the latitude, altitude and conditions, as predicted by Shiraiwa *et al.*[31] Our first goal is to understand the effect of RH on the photodegradation of SOA compounds, which have not been previously explored in experiments. The results described below suggest that the photodegradation rate estimates based on previous measurements under dry conditions may be too conservative.[16]

Iron is emitted into the troposphere as minerals, as amorphous hydroxides, such as $Fe(OH)_3$, adsorbed on clay minerals, organic matter, or carbonaceous particles or bound in salts. It may be released from the particulate form by complexation or acidic dissolution into the aqueous phase.[32,33] Dissolved iron is present in the atmosphere in two oxidation states, (II) and (III), which interconvert by various redox processes. The work of Wang *et al.*[34] indicates that the iron can be highly concentrated in continental aerosol particles near the surface of the Earth. For instance, in Europe the observed concentrations of iron are between 0.1–1 μg m^{-3} (~0.8–8% in molar ratio in SOA). A study from Moffet *et al.* (2012) has shown that in urban outflow, all particles have organic matter dominated by carboxyl functionalities, and, among them, 5% contain detectable Fe.[35] In the technique they used, the detection limit was about 5% of iron in molar ratio. Saharan dust, urban particles, coal fly ash and oil fly ash contain iron in the range from 3 to 9% by weight.[33] The fraction of soluble Fe in desert dust typically goes from values ~0.1% to up to ~80%.[36–38] On the other hand, measurements of dissolved iron in rural or urban atmospheric waters indicate concentrations ranging from 10^{-7} up to 10^{-2} M. Overall, dissolved iron concentrations in aerosol particles vary broadly and typically range from micromolar to millimolar levels.

Depending on chemical parameters such as ionic strength, pH and concentration of involved compounds, iron is present in the form of complexes with the organic and inorganic compounds in the aerosol particles and cloud droplets.[33] Some of these complexes have strong ligand-to-metal charge transfer (LMCT) bands in the UV and visible ranges of the solar spectrum. Excitation of these LMCT bands in Fe(III) complexes leads to photoreduction of iron to Fe(II) and decomposition of the ligands by free radical chemistry. Fe(III)–carboxylate complexes are well-known photoactive compounds in atmospheric aerosol particles which drive LMCT transitions leading to the decarboxylation of the ligands, being the major particle phase sink of carboxylate groups in the atmosphere.[9] Even if SOM is not light-absorbing by itself it can become photodegradable in presence of soluble Fe because of these LMCT transitions. The degradation of the carboxylic groups is followed by the production of OVOCs and CO_2,[39,40] which contribute to the particle mass loss. Iron can cycle between Fe(II) and Fe(III) through HO_x radicals and H_2O_2 chemistry due to several redox reactions[8] such as Fenton reactions. Fig. 1 shows some of the key processes involved in photochemistry of Fe/SOM mixtures, which may produce OVOCs by various mechanisms including direct photolysis or reactions with HO_x radicals, the iron redox chemistry with HO_x radicals and H_2O_2 and the photochemistry of iron carboxylates, which produce additional OVOCs.

A number of studies have provided evidence for the photochemical reactions between soluble iron and organic compounds found in atmospheric particles. Wentworth and coworkers used IR spectroscopy to demonstrate that complexes of Fe(III) with gallic acid can be photolyzed, degrading gallic acid to quinones and further to OVOCs.[41] It has been found that the reactive uptake of glycolaldehyde can be induced by OH radicals produced by Fe(III) oxalate complex photolysis. At the same time, the degradation of iron complexes produces enough OVOCs to prevent aerosol growth by uptake of glycoaldehyde,[42,43] showing competition between accretion and fragmentation. Styler *et al.*[44] showed that mineral dust particles doped with oxalate can release CO_2 by photolysis, mediated by LMCT, of Fe(III)–oxalate complexes. Weller *et al.*[39] found that the photolysis of Fe(III) carboxylate complexes, such as iron oxalate, pyruvate or glyoxalate, is a

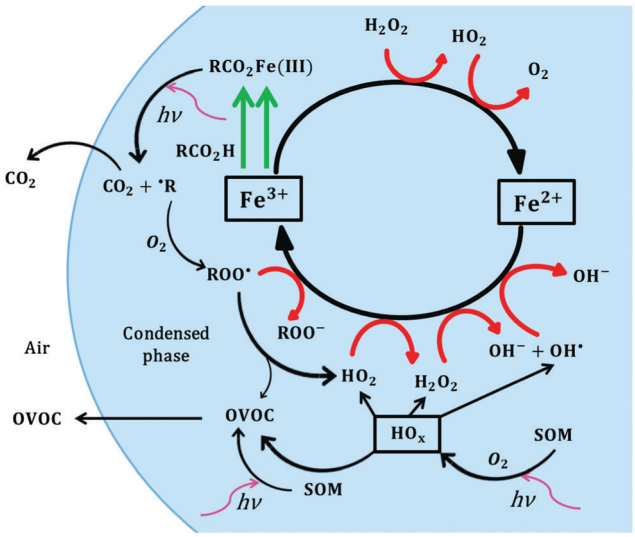

Fig. 1 Photochemical mechanisms of degradation of SOM mediated by iron photochemistry and radical chemistry coupled with iron cycling induced by HO_x radical chemistry.

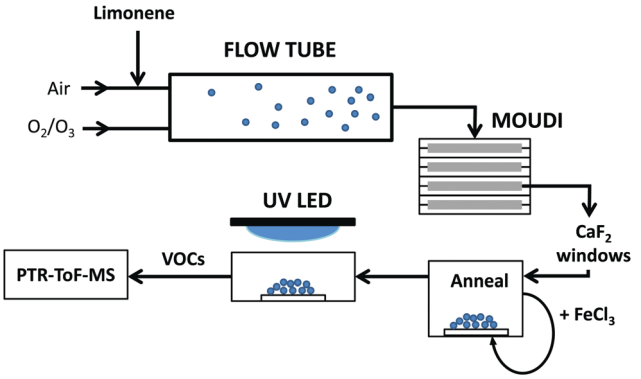

Fig. 2 Diagram illustrating SOM preparation and UV exposure steps. SOA particles are produced by mixing a flow of air and O_2/O_3 with D-limonene in a flow tube. The particles are collected on CaF_2 windows located in a MOUDI, and the particles are annealed. $FeCl_3$ is added for the iron content dependence experiments. After annealing at 40 °C, samples are irradiated with a 305 nm UV-LED, and the OVOCs released are analyzed by a PTR-ToF-MS.

significant source of HO_x radical production and the main sink of carboxylic acids in aerosol particles.

The second goal of this work is to study how the presence of Fe(III) influences the OVOC release from SOA particles. SOA produced by oxidation of VOCs contain hundreds of different compounds, and some of them may have strong affinity for dissolved Fe and also form complexes with it. The compounds in SOA are known to slowly photodegrade in the presence of UV radiation releasing OVOCs, such as formic acid, acetic acid, acetaldehyde and acetone.[16] Our initial hypothesis was that the photodegradation rate would be enhanced because of the LMCT transitions in complexes between Fe and SOA compounds. In fact, an enhancement of the OVOC release is only observed for low Fe(III) concentrations in SOA, but, as we show below, the photochemistry is actually suppressed at higher Fe(III) concentration demonstrating a potentially complicated role of Fe(III) on SOA photochemistry.

Experimental section

A diagram illustrating the SOA preparation and irradiation experiments is shown in Fig. 2. SOA was generated by oxidation of D-limonene (Sigma-Aldrich, 98%) with ozone in a ~20 L Plexiglas flow cell in the absence of seed particles. No particles were produced in control experiments with only ozone flowing through the cell, without D-limonene added. Pure oxygen at 0.5 L min^{-1} was sent through an ozone generator and into the flow cell. Limonene was evaporated in a separate 4.5 L min^{-1} air flow using a syringe pump at 25 μL per hour liquid flow rate. The flow of air containing limonene was mixed with the O_3/O_2 flow at the entrance of the flow cell. The starting mixing ratios of ozone and limonene were about 20 ppm and 10 ppm, respectively, and the reaction time in the flow cell was about 4 min.

Particles were collected with a Micro-Orifice Uniform-Deposit Impactor (MOUDI, MSP Corp. model 110-R) equipped with custom-made metal supporting rings to accommodate 2.54 cm diameter CaF_2 windows as substrates instead of Teflon or foil filters. We typically collected hundreds of micrograms of SOM per window; the largest amount was typically found on stages 8 (0.18–0.32 μm particle size range) and 9 (0.10–0.18 μm particle size range), and these samples were used for the experiments. In our previous experiments with D-limonene ozonolysis SOA, we found no dependence of SOA particle chemical composition on particle size in the 0.05 to 0.5 μm range,[45] so we used samples collected on stages 8 and 9 interchangeably. The window was then placed in a laboratory oven overnight at 40 °C with ~10 L min^{-1} of purge air flowing over it in order to drive off higher volatility species and help anneal the collected SOA particles into a more uniform SOM film on the window. The main justification for this "annealing" procedure is that SOA produced by the ozonolysis of alkenes contains unstable peroxide molecules that decompose on a time scale of hours.[10,46] This decomposition produces volatile products that would interfere with the detection of volatiles produced in the photodegradation experiments described below.[16] In addition, semi-volatile species that partitioned into aerosol particles because of the unrealistically high concentrations in the flow tube have a chance to evaporate making the volatility distribution of SOA compounds more compatible with that of ambient aerosol particles. The annealed SOA samples can therefore be regarded as particles that have been aged *via* spontaneous decomposition of peroxides but not by photochemical processes. For the RH dependent experiments, we used the sample immediately after annealing without further adjustments.

For the experiments with variable amounts of Fe(III), a certain volume ranging from 50 μL to 2000 μL of a solution of $FeCl_3$ in water (0.001 M, pH = 5) was dropped on the window surface, and the sample was placed again in the laboratory oven overnight under the same conditions as before.[16] We elected to use $FeCl_3$ as the Fe(III) source because it is highly soluble.

While chloride anions are not chemically inert and could be converted into chlorine atoms in reaction with OH, chloride anions are ubiquitous in atmospheric particles, and it is reasonable to have them as part of the mixture. Even so, the rate coefficient for the reaction between chloride and OH radicals[47] is around one order of magnitude smaller than the one for the reaction between a usual SOA organic compound and OH. Therefore the interference should be negligible. For larger volumes from 1000 μL up to 2000 μL, the solution was applied in two additions to avoid spilling over the edges of the window. For volumes lower than 500 μL, an additional droplet of water was added up to 500 μL to be sure that the solution covered the entire window. For the control experiments, 500 μL of nanopure water was used instead of the Fe-containing solution. The addition of liquid resulted in a redistribution of SOM on the CaF_2 window, resulting in a reduction in the film thickness in the center and a build-up of the material on the edges. The material was redistributed due to an outflow created within the droplet while it was evaporating due to the different evaporation rate in the edge compared with the one on the top of the deposited droplet.[48] (In retrospect, it might have been better to prepare the samples differently, for example by re-aerosolizing an aqueous solution of Fe(III) mixed with dissolved SOM and collecting the resulting particles. Such experiments are planned for the future.) Because the CaF_2 window was always fully covered by the deposited droplet, we assume that the fraction exposed to UV light was always the same for every experiment and that the ratio Fe(III)/SOM is homogeneous through the sample after drying. Experiments with identical conditions of Fe(III) concentration, irradiation and RH did not indicate a dependence of OVOCs release on the volume of solution used to deposit Fe(III).

The window was then placed into a custom-made glass flow cell with 0.2 L min^{-1} of purge air flowing over the window. A UV-light emitting diode (Thorlabs, Inc. model M300L4) with a wavelength centered at ~305 nm, a full width half-maximum of ~10 nm, and a power of 26 mW at 350 mA current (measured with a Coherent Powermax PS19Q power sensor) was used to irradiate the particles on the CaF_2 window. Based on the amount of the deposited material, and known mass absorption coefficients of D-limonene ozonolysis SOA,[49] we estimated that the samples were optically thin, so the UV intensity was approximately the same throughout the thickness of the sample. Although the sample distribution on the surface was not uniform, as ascertained by the examination of the sample under a microscope, all the material on the window was accessible to the UV radiation. For the experiments with variable iron content dependence, the exposures to UV light were made either under dry air conditions or at 55 ± 2% RH (measured with a Vaisala HMP330 humidity probe). For the experiments related to the RH dependence of SOM decomposition, in which no Fe(III) was added to the SOM sample, we exposed SOM to UV radiation under a wider range of RH values.

OVOCs in the flow exiting the photolysis cell were detected by a Proton Transfer Reaction Time-of-Flight Mass Spectrometer (PTR-ToF-MS). Standard ion source conditions were used: E/N = 130–135 Td, U_{drift} = 600 V, T_{drift} = 60 °C, and P_{drift} ~ 2.2 mbar. The PTR-ToF-MS was previously calibrated under the same ion sources conditions with respect to several OVOCs, namely acetic acid, formic acid, acetone and acetaldehyde by injecting known amounts of these compounds in a 5 m^3 chamber, similar to a procedure described in Malecha and Nizkorodov.[16] For experiments at different RH the signal was normalized to take into account the RH dependence of the ion detection sensitivity. Specifically, we evaluated the variation of the ionizing agents (H_3O^+ and $H_3O^+(H_2O)$) with respect to the experiments at dry conditions and we normalized the signal to those. We took into account the different reactivity that the two ionizing agents have with the VOCs.[50,51] Additional details are provided in the ESI.†

Results and discussion

Fig. 3 shows PTR-ToF mass spectra of the air passing over the SOM before and during the UV irradiation. Upon irradiation, certain peaks increase indicating the production and release of the corresponding compounds from SOM. The major peaks that increase are detected at *m*/*z* 43.055 (ketene, ethynol, or oxirene), *m*/*z* 45.034 (acetaldehyde), *m*/*z* 47.013 (formic acid), *m*/*z* 59.050 (acetone, propanal, or allyl alcohol) and *m*/*z* 61.029 (acetic acid, glycoaldehyde, or methyl formate). Because of the inability of PTR-ToF-MS to distinguish structural isomers, the assignments cannot be made with certainty. However, because of chemical considerations about the possible mechanism of degradation, the *m*/*z* 45.034, 47.013, 59.050, and 61.029 peaks are assigned to acetaldehyde, formic acid, acetone and acetic acid, respectively. The peak at *m*/*z* 43.055 is likely a fragment of acetic acid.[52]

Photolysis processes such as bond cleavage into free radicals, photoisomerization, H abstraction or photosensitization,[2]

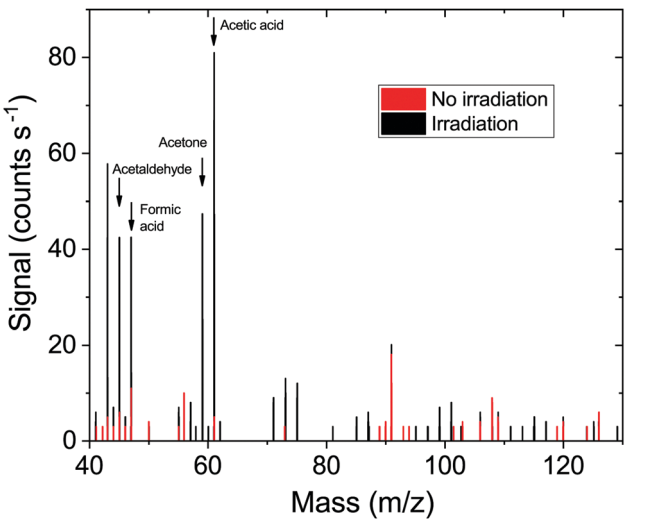

Fig. 3 PTR-ToF-MS stick spectra of the OVOCs released from SOM at 0% RH, in the absence of iron before (red) and 10 minutes after starting irradiation (black) irradiation. The peaks of the OVOCs discussed in the paper are indicated by arrows.

together with HO_x radical reactions, are the processes controlling the OVOC production. For example, acetone could be a product of degradation by Norrish type-II mechanisms, *i.e.*, splitting of methyl terminated ketones. Acetic acid and formic acid could be produced by direct photolysis or by reaction of organics with HO_x radicals, which will react with organics by hydrogen abstraction and oxidation reactions which can lead to the cleavage of carbon chains. Additionally we rely on the LMCT reactions of iron complexes as additional source of CO_2 and OVOC by decarboxylation and further degradation of the organic radicals initially produced.

Effect of RH on samples without added Fe(III)

Fig. 4a shows the signal of acetaldehyde observed at different RH values. For ease of comparison, the signal was normalized to the maximal steady-state signal achieved during irradiation. The release of acetaldehyde levels off after about 15 minutes for dry conditions but the time needed to achieve the steady state becomes shorter for the experiments at higher RH (4 minutes for 70% RH). We attribute this faster time to establish steady state release of acetaldehyde at higher RH to an increased diffusion coefficient for acetaldehyde through SOM. (While we attribute our observations to the diffusion effects, we cannot exclude changes in the photochemical mechanisms arising, for example, from the hydrolysis of organic compounds at high RH.) The increased diffusivity would be caused by the decrease of viscosity with increasing water content in the film. Indeed, the viscosity of SOM prepared by ozonolysis of α-pinene[53] and D-limonene[29] has been shown to decrease with RH. The reported self-diffusion coefficients in SOM change widely with RH[22–24] going from 10^{-22}–10^{-20} cm^2 s^{-1} at dry conditions to 10^{-9}–10^{-7} cm^2 s^{-1} at high RH (80–90% RH) while the diffusion coefficient of water in α-pinene SOA varies from 10^{-11}–10^{-10} cm^2 s^{-1} at dry conditions to 10^{-8}–10^{-6} cm^2 s^{-1} at high RH.

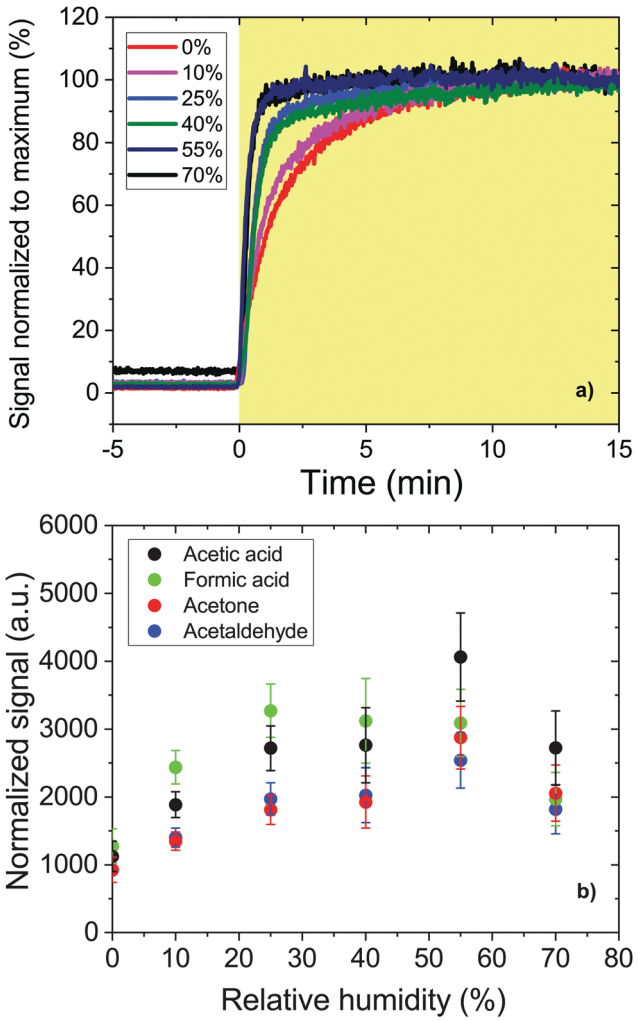

Fig. 4 (a) Signal of acetaldehyde normalized to the maximum of the signal for each sample upon irradiation (shaded zone) at several values of RH. (b) Signal of OVOCs upon UV irradiation corresponding to the total OVOC flux and multiplied by the flow in mL min^{-1} for SOM samples *versus* relative humidity (%). The error bars represent the standard deviation resulting from 2 or 3 experiments.

Fig. 4b shows the dependence of release of several OVOCs on RH. Each data point is the average of 2 or 3 replica experiments. Because the ionization efficiency of certain low-proton-affinity VOCs (such as benzene,[54] monoterpenes,[55] and formaldehyde[56]) are sensitive to RH, we corrected for the RH-dependent ionization efficiency in the PTR as described in the ESI.† For the species of interest, these corrections were very small. In the data shown in Fig. 4b, the signal was normalized by the total mass of the SOM assuming that the amount of emitted OVOC should be directly proportional to the SOM mass (the SOM samples were optically thin, so such normalization is appropriate). The signal was further multiplied by the total gas flow through the sample in order to correct for the dilution with different gas flows used in different experiments. With this normalization method, the magnitude of the normalized signal is proportional to the actual OVOC flux out of the material. The data were taken from the time period where the release reaches the maximum which was different for different humidity conditions, as shown in Fig. 4a.

The release of every compound shown in Fig. 4b increases with RH from 0% to 40–55% RH. There are two possible explanations for this. Firstly, certain photochemical reactions are suppressed in viscous SOA, especially the ones involving secondary reactions of long-lived electronically excited molecules.[29] Secondly, since it takes OVOCs longer to diffuse through the SOM at lower RH, the probability that they are degraded by secondary free-radical driven reactions before they get out of the material increases.

From 55% RH to 70% RH the rate of OVOC release appears to decrease by more than 25% (although we have only one data point that shows this trend). This could be a result of a dilution effect: as the water activity in the SOM increases the concentrations of all other reactants decrease. Based on the work of Virkkula and coworkers,[57] the concentration of water in D-limonene SOA goes up to 7 M at 80% RH, and it could be even higher in the presence of hygroscopic $FeCl_3$. Previous research has shown that oxygen solubility in organic solvents, such ethanol, propanol or carboxylic acids, is higher than in water.[58] Therefore, we assume that oxygen solubility also decreases upon increasing

water activity meaning that HO_x radicals deriving from photolysis of SOM will be produced less efficiently because the precursor molecule (O_2) is less concentrated and subsequently OVOC production will be decreased. (HO_x radicals could also be produced by the photolysis of peroxides in D-limonene ozonolysis SOM but the lifetime of peroxides in this SOM is known to be around 6 hours,[46] so most of them should be already degraded by the annealing procedure done before the measurement.) The decrease of the concentration of both organic reactants and oxygen at higher RH should result in a decrease of second order reaction rates. Thus, the OVOC release is expected to get smaller with increasing RH. Similar dependence on RH, featuring a maximum at certain RH level, was observed in the HO_2 release in previous work.[4]

We estimated the diffusion coefficient of acetaldehyde at different values of RH based on the decay of its concentration in the flow after switching off the UV light (Fig. 5). We developed a kinetic multi-layer model by means of the diffusion eqn (1), which provides a depth-resolved description of mass transport and release in films as a function of time, dividing our film in 30 equally thick layers. A detailed description of the model is provided in the ESI.† The diffusion is considered throughout the film by applying the diffusion equation to every layer. Because the gas flow over the film is fast (on the order of hundreds of mL per minute), we assume that the gas phase concentration of acetaldehyde next to the surface plays no role in the equilibrium between condensed and gas phase. Therefore, the release is described as the diffusion into a gas layer, where the concentration is negligible. We estimated the thickness of the sample assuming that the density of the SOM is 1.5 g cm^{-3}.[59]

$$\frac{\partial C}{\partial t} = D\frac{\partial^2 C}{\partial x^2} \quad (1)$$

We optimized the values of the diffusion coefficients at different RH by fitting the release predicted by the model to the observed decay of acetaldehyde after switching off lights as shown in Fig. 5a. We note that the initial concentration profile in the film may change the release. Therefore, we tested the sensitivity of two initial concentration profiles on the diffusion coefficient parameter to reproduce our data: (i) uniform initial concentration profile is flat throughout the film (which is consistent with the optically thin samples used in this work, with the UV radiation penetrating through the entire film) and (ii) linear initial concentration profile where its maximum concentration is at the bottom of the film and zero at the surface (a conceivable scenario after prolonged irradiation). These two different scenarios should provide a lower (i) and upper (ii) limit set of predicted diffusion coefficients respectively.

The trend of the calculated diffusion coefficients follows the expected trend, *i.e.*, diffusion coefficients increasing with RH. The calculated upper limit diffusion coefficients of acetaldehyde are two or three orders of magnitude at low RH and four or five orders of magnitude at high RH lower than the diffusion coefficients of water in alpha-pinene SOA measured previously by Lienhard *et al.*[60] as showed in Fig. 5. The molecule of acetaldehyde is larger than the molecule of water so, based on the

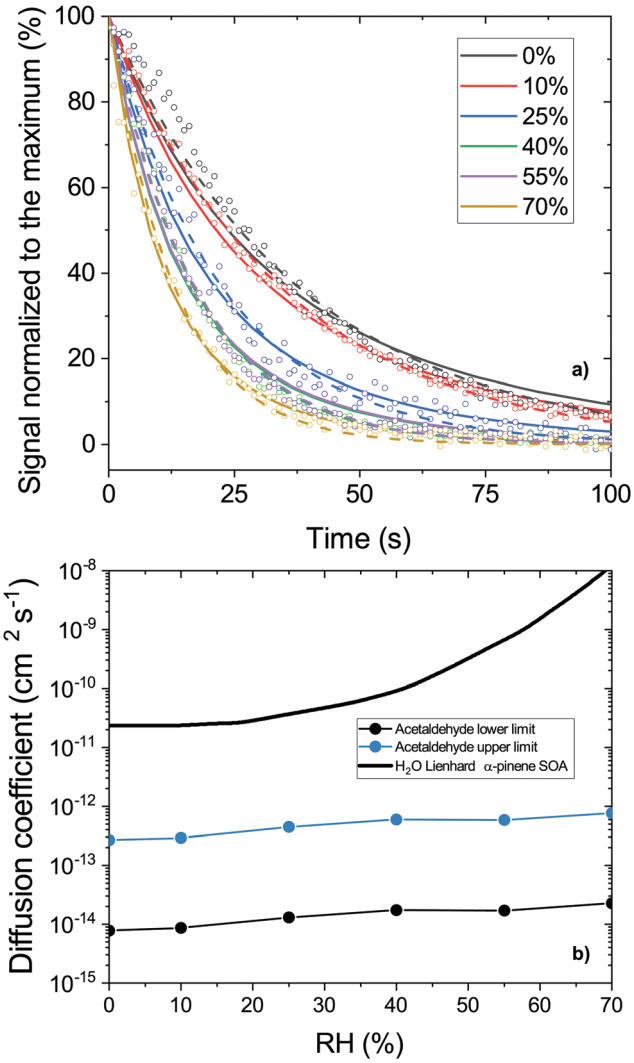

Fig. 5 (a) Signal of acetaldehyde after irradiation background-subtracted and normalized to the maximum of the signal for each sample upon irradiation (symbols) as a function of RH. Predictions by the diffusion model with upper and lower limits for the diffusion coefficient are shown as dashed and solid lines, respectively. (b) Diffusion coefficients predicted by the model for acetaldehyde as a function of RH, with the upper (blue) and lower (black) limits shown as blue and black symbols, respectively. The black line corresponds to the water diffusion coefficient in α-pinene SOA as measured by Lienhard *et al.*[60]

Stokes–Einstein equation, we would expect water to diffuse only around two times faster than acetaldehyde. However, the Stokes–Einstein equation performs poorly for molecules of this size,[61] so quantitative comparison is not possible. But as the upper limit values for the acetaldehyde diffusion coefficients in Fig. 5 are closer to the reported values for water, they are probably more representative of the actual diffusion coefficients. The relative change of D between 0 and 70% RH is a factor of 2–3 while a range of about one or two orders of magnitude is observed for D_{H_2O} in SOA[60,62] and a range of about 9 to 10 orders of magnitude is observed for D_{org} in sucrose.[63] A possible explanation for this would be that the steady-state profile of the concentration of acetaldehyde in limonene SOA while irradiation is

flat at low RH (lower limit prediction) and it will have a gradient at high RH (upper limit prediction). This latter situation will lead to a difference of D of about two orders of magnitude from low RH and high RH.

Effect of added Fe(III)

Fig. 6 shows the PTR-ToF-MS time-dependent signal of acetic acid released under irradiation under dry conditions (a) and at 55% RH (b). The signal was normalized by the initial dry mass of SOM on the substrate (it was not corrected for the RH-dependent ionization efficiency because only signals at the same RH are compared to each other). Different traces correspond to different mole fractions of added Fe(III) (estimated assuming an average molar mass of 200 g mol^{-1} for SOM compounds). The release reaches a maximum around 30 minutes after the start of the irradiation, and after that the release drops slowly, and finally drops to the baseline level after several hours of UV exposure (not shown). At 55% RH, the maximum signal is reached earlier than under dry conditions because the diffusion of the OVOCs through SOM is faster at higher RH, as discussed above, and the steady state release is reached earlier. The release of other compounds (acetaldehyde, formic acid, and acetone) shows the same trend as acetic acid.

Fig. 7 shows the average of the normalized signal of the 4 OVOCs under dry conditions (a) and at 55% RH (b). To account for the faster appearance of the signal in humidified air, the averaging period is 2000–2500 s (33.3–46.7 min) for dry conditions, and 750–1000 s (12.5–16.7 min) at 55% RH. Contrary to our expectations that the presence of Fe should accelerate photodegradation of SOM, there is a general decreasing trend in the signal of OVOC photoproducts with the relative amount of added Fe. This overall decreasing trend cannot be explained by the differences in the absorption coefficients of the samples because the samples were in fact more absorbing at higher Fe fractions (however, we have not corrected for the change in the absorption coefficient in this work). The trend is not linear, however. At 55% RH, the release of all OVOC is higher for samples with 4% of Fe(III) compared to samples without

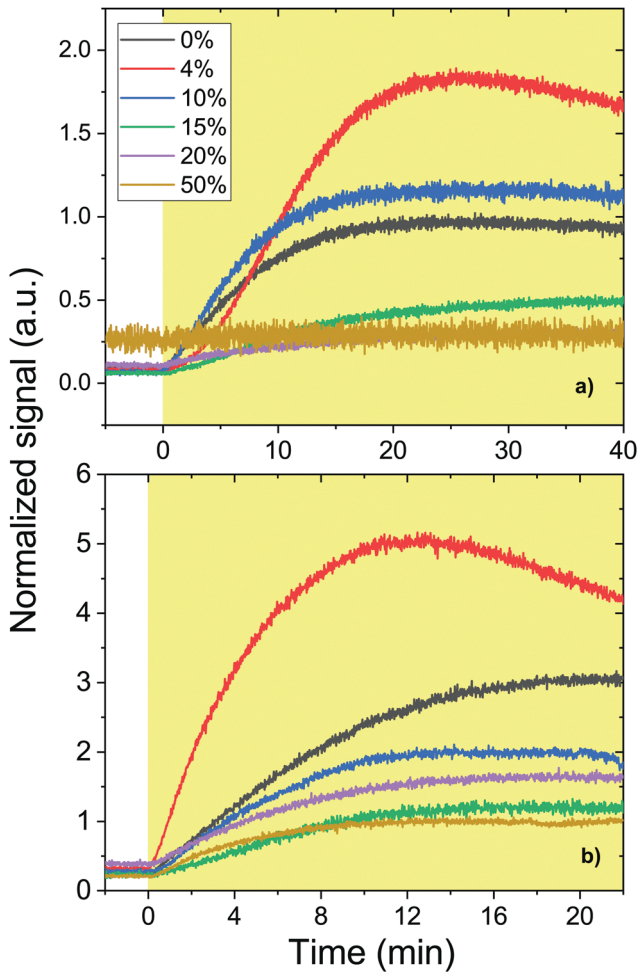

Fig. 6 PTR-ToF-MS signal of acetic acid released upon UV irradiation for SOM samples *versus* time at different mole fractions of added $FeCl_3$ (specified with % values in each panel) under dry conditions (a) and at 55% RH (b). The yellow-shaded zone indicates the irradiation time. Signals from different samples were normalized to the total mass of the sample.

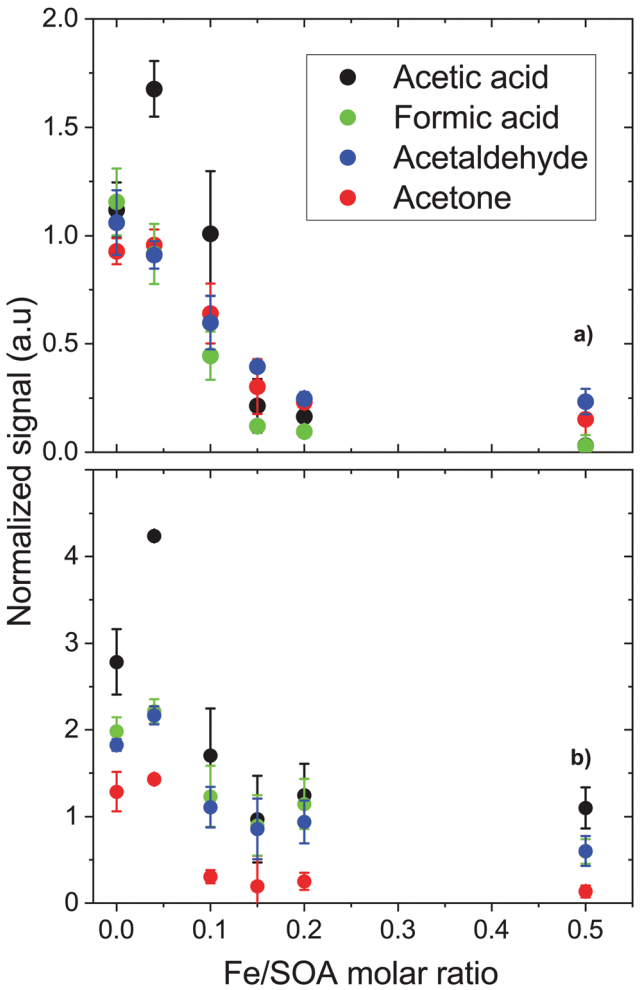

Fig. 7 Peak intensities of signals from acetic acid, formic acid, acetaldehyde and acetone normalized to the total mass of the sample for SOM samples *versus* Fe/SOA molar ratio under dry conditions (a) and at 55% RH (b). The error bars represent the standard deviation resulting from 2 or 3 repeated experiments.

added Fe. Above that fraction (and above 10% for acetone and acetic acid), OVOC release drops below that of SOM without Fe added. Then at higher Fe(III) concentrations, the release is strongly suppressed. Under dry conditions, acetic acid and perhaps acetone follow a similar trend with a maximum emission at 4% Fe(III), and decreasing at higher Fe(III) concentrations. For acetaldehyde and formic acid there is a steady decrease of the signal as the Fe(III) concentration is increasing. At 55% RH, all species exhibit first increased release with increasing Fe(III) content, and then a decrease for higher Fe(III) additions. We suspect that two competing effects may be at work, one enhancing the OVOC release at low Fe(III) concentrations and suppressing it at high Fe(III) concentrations.

The enhancement in the release of OVOCs at low Fe(III) concentrations may result from increased OVOC production from the photolysis of iron carboxylate complexes likely produced after adding Fe(III) to SOM, as illustrated in Fig. 1. This is in agreement with the work of Hems *et al.*[64] which found that the OH production from the photodegradation of SOA compounds by themselves is slower than the one promoted by iron carboxylate complexes formed between iron and SOA material at low Fe/SOA ratio ($\sim$0.3%). The enhancement in OVOC release can be due to (i) increase of the HO_x radical production inside SOM and (ii) the direct photolysis of iron carboxylate complexes. We also cannot discard a possibility that the chloride anions present in the samples are not playing a role in the photochemistry – they could potentially be converted into highly reactive chlorine atoms by reactions with OH inside SOM. Our experiments cannot differentiate between these possibilities.

The decrease of the OVOC release at high iron concentration may be the result of the presence of incompletely complexed Fe in the condensed phase, *i.e.*, not with all coordination sites occupied by the SOA carboxylic ligands. Instead of driving LMCT transitions, incompletely complexed iron could be cycling between Fe(III) and Fe(II) (Fig. 1) turning HO_x radicals into water and oxygen and making them unavailable to oxidize SOA compounds into OVOCs.

Conclusions and atmospheric implications

This work reveals that RH will play an important role in the OVOC release from SOA induced by photolysis of the compounds presents in SOA. In the work of Malecha and Nizkorodov (2016), they estimated the emission of OVOC coming from the photolysis of several SOA under dry conditions and they predicted that SOA particles may lose at least $\sim$1% of their mass over 24 hours during summertime conditions in Los Angeles, California. We claim that, under more realistic relative humidity conditions ($\sim$50%), the mass loss experienced by SOA particles may be up to 2 to 4 times higher than what was estimated in the work of Malecha and Nizkorodov.[16] We propose that all future photodegradation studies of SOA should be done under humid conditions to more accurately estimate the rate of mass loss from the particles. To explain the assumption that D varies over several orders of magnitude while increasing RH from 0% to 70%, we suggest the presence of OVOCs concentration gradients taking place over a range of hundreds of nanometers in aerosol particles during photolysis. When photolysis rates are not too high, these gradients are presumably kept in a situation close to steady-state in atmospheric aerosol particles but they can develop while the particles age. Their spatial extent depends on humidity conditions, nature of the SOM and nature of the diffusing molecule. The diffusion coefficient of acetaldehyde in limonene SOA in the range from 10^{-14} to 10^{-12} cm^2 s^{-1}.

The second conclusion of this work is that iron influences the OVOC generation and release during UV irradiation of SOA particles. For atmospherically relevant conditions of humidity and iron content (up to 4% of iron molar ratio), OVOC release will be slightly enhanced likely due to the efficient photo-degradation of iron carboxylate complexes. At higher iron content a surprising suppression of the photodegradation is observed, although such high concentrations are unlikely in realistic atmospheric particles. As described in the introduction, dissolved iron concentrations in aerosol particles vary broadly and range from micromolar up to an upper limit of about 10%. Our findings point out that OVOC production and release is strongly influenced by iron in iron-containing particles, with the sign and magnitude of the effects being dependent on the concentration and conditions.

Conflicts of interest

The authors declare no competing financial interests.

Acknowledgements

We would like to thank Peter A. Alpert for helpful discussions and support. P. C. A. and M. A. appreciate support by the Swiss National Science Foundation (grant no. 163074). K. T. M. thanks the National Science Foundation (NSF) for support from the Graduate Research Fellowship Program. S. A. N. thanks a grant from the US Department of Energy (DE-SC0018349) for the support. The PTR-ToF-MS was acquired with the NSF grant MRI-0923323.

References

1 U. Poschl, Atmospheric aerosols: composition, transformation, climate and health effects, *Angew. Chem.*, 2005, **44**(46), 7520–7540.
2 C. George, M. Ammann, B. D'Anna, D. J. Donaldson and S. A. Nizkorodov, Heterogeneous Photochemistry in the Atmosphere, *Chem. Rev.*, 2015, **115**(10), 4218–4258.
3 M. Shiraiwa, L. D. Yee, K. A. Schilling, C. L. Loza, J. S. Craven, A. Zuend, P. J. Ziemann and J. H. Seinfeld, Size distribution dynamics reveal particle-phase chemistry in organic aerosol formation, *Proc. Natl. Acad. Sci. U. S. A.*, 2013, **110**(29), 11746–11750.
4 L. González Palacios, P. Corral Arroyo, K. Z. Aregahegn, S. S. Steimer, T. Bartels-Rausch, B. Nozière, C. George, M. Ammann and R. Volkamer, Heterogeneous photochemistry

of imidazole-2-carboxaldehyde: HO_2 radical formation and aerosol growth, *Atmos. Chem. Phys.*, 2016, **16**(18), 11823–11836.

5 C. M. Sharpless and N. V. Blough, The importance of charge-transfer interactions in determining chromophoric dissolved organic matter (CDOM) optical and photochemical properties, *Environ. Sci.: Processes Impacts*, 2014, **16**(4), 654–671.

6 J. D. Smith, V. Sio, L. Yu, Q. Zhang and C. Anastasio, Secondary organic aerosol production from aqueous reactions of atmospheric phenols with an organic triplet excited state, *Environ. Sci. Technol.*, 2014, **48**(2), 1049–1057.

7 K. Z. Aregahegn, B. Noziere and C. George, Organic aerosol formation photo-enhanced by the formation of secondary photosensitizers in aerosols, *Faraday Discuss.*, 2013, **165**, 123–134.

8 H. Herrmann, B. Ervens, H. W. Jacobi, R. Wolke, P. Nowacki and R. Zellner, CAPRAM2.3: a chemical aqueous phase radical mechanism for tropospheric chemistry, *J. Atmos. Chem.*, 2000, **36**(3), 231–284.

9 C. Weller, A. Tilgner, P. Brauer and H. Herrmann, Modeling the impact of iron-carboxylate photochemistry on radical budget and carboxylate degradation in cloud droplets and particles, *Environ. Sci. Technol.*, 2014, **48**(10), 5652–5659.

10 M. Krapf, I. El Haddad, E. A. Bruns, U. Molteni, K. R. Daellenbach, A. S. H. Prevot, U. Baltensperger and J. Dommen, Labile Peroxides in Secondary Organic Aerosol, *Chem*, 2016, **1**(4), 603–616.

11 S. A. Mang, D. K. Henricksen, A. P. Bateman, M. P. S. Andersen, D. R. Blake and S. A. Nizkorodov, Contribution of carbonyl photochemistry to aging of atmospheric secondary organic aerosol, *J. Phys. Chem. A*, 2008, **112**(36), 8337–8344.

12 K. M. Henry and N. M. Donahue, Photochemical Aging of alpha-Pinene Secondary Organic Aerosol: Effects of OH Radical Sources and Photolysis, *J. Phys. Chem. A*, 2012, **116**(24), 5932–5940.

13 D. E. Romonosky, Y. Li, M. Shiraiwa, A. Laskin, J. Laskin and S. A. Nizkorodov, Aqueous Photochemistry of Secondary Organic Aerosol of alpha-Pinene and alpha-Humulene Oxidized with Ozone, Hydroxyl Radical, and Nitrate Radical, *J. Phys. Chem. A*, 2017, **121**(6), 1298–1309.

14 A. P. Bateman, S. A. Nizkorodov, J. Laskin and A. Laskin, Photolytic processing of secondary organic aerosols dissolved in cloud droplets, *Phys. Chem. Chem. Phys.*, 2011, **13**(26), 12199–12212.

15 J. H. Kroll, J. D. Smith, D. L. Che, S. H. Kessler, D. R. Worsnop and K. R. Wilson, Measurement of fragmentation and functionalization pathways in the heterogeneous oxidation of oxidized organic aerosol, *Phys. Chem. Chem. Phys.*, 2009, **11**(36), 8005–8014.

16 K. T. Malecha and S. A. Nizkorodov, Photodegradation of Secondary Organic Aerosol Particles as a Source of Small, Oxygenated Volatile Organic Compounds, *Environ. Sci. Technol.*, 2016, **50**(18), 9990–9997.

17 K. E. Daumit, A. J. Carrasquillo, R. A. Sugrue and J. H. Kroll, Effects of Condensed-Phase Oxidants on Secondary Organic Aerosol Formation, *J. Phys. Chem. A*, 2016, **120**(9), 1386–1394.

18 J. P. S. Wong, S. M. Zhou and J. P. D. Abbatt, Changes in Secondary Organic Aerosol Composition and Mass due to Photolysis: Relative Humidity Dependence, *J. Phys. Chem. A*, 2015, **119**(19), 4309–4316.

19 S. A. Epstein, S. L. Blair and S. A. Nizkorodov, Direct Photolysis of a-Pinene Ozonolysis Secondary Organic Aerosol: Effect on Particle Mass and Peroxide Content, *Environ. Sci. Technol.*, 2014, **48**(19), 11251–11258.

20 X. Pan, J. S. Underwood, J. H. Xing, S. A. Mang and S. A. Nizkorodov, Photodegradation of secondary organic aerosol generated from limonene oxidation by ozone studied with chemical ionization mass spectrometry, *Atmos. Chem. Phys.*, 2009, **9**(12), 3851–3865.

21 M. L. Walser, J. Park, A. L. Gomez, A. R. Russell and S. A. Nizkorodov, Photochemical aging of secondary organic aerosol particles generated from the oxidation of D-limonene, *J. Phys. Chem. A*, 2007, **111**(10), 1907–1913.

22 T. Berkemeier, S. S. Steimer, U. K. Krieger, T. Peter, U. Poschl, M. Ammann and M. Shiraiwa, Ozone uptake on glassy, semi-solid and liquid organic matter and the role of reactive oxygen intermediates in atmospheric aerosol chemistry, *Phys. Chem. Chem. Phys.*, 2016, **18**(18), 12662–12674.

23 Y. C. Song, A. E. Haddrell, B. R. Bzdek, J. P. Reid, T. Bannan, D. O. Topping, C. Percival and C. Cai, Measurements and Predictions of Binary Component Aerosol Particle Viscosity, *J. Phys. Chem. A*, 2016, **120**(41), 8123–8137.

24 D. M. Lienhard, A. J. Huisman, D. L. Bones, Y. F. Te, B. P. Luo, U. K. Krieger and J. P. Reid, Retrieving the translational diffusion coefficient of water from experiments on single levitated aerosol droplets, *Phys. Chem. Chem. Phys.*, 2014, **16**(31), 16677–16683.

25 Q. Ye, E. S. Robinson, X. Ding, P. Ye, R. C. Sullivan and N. M. Donahue, Mixing of secondary organic aerosols versus relative humidity, *Proc. Natl. Acad. Sci. U. S. A.*, 2016, **113**(45), 12649–12654.

26 M. Shiraiwa, M. Ammann, T. Koop and U. Poschl, Gas uptake and chemical aging of semisolid organic aerosol particles, *Proc. Natl. Acad. Sci. U. S. A.*, 2011, **108**(27), 11003–11008.

27 J. H. Slade and D. A. Knopf, Multiphase OH oxidation kinetics of organic aerosol: the role of particle phase state and relative humidity, *Geophys. Res. Lett.*, 2014, **41**(14), 5297–5306.

28 T. Yli-Juuti, A. Pajunoja, O. P. Tikkanen, A. Buchholz, C. Faiola, O. Vaisanen, L. Q. Hao, E. Kari, O. Perakyla, O. Garmash, M. Shiraiwa, M. Ehn, K. Lehtinen and A. Virtanen, Factors controlling the evaporation of secondary organic aerosol from alpha-pinene ozonolysis, *Geophys. Res. Lett.*, 2017, **44**(5), 2562–2570.

29 M. L. Hinks, M. V. Brady, H. Lignell, M. J. Song, J. W. Grayson, A. K. Bertram, P. Lin, A. Laskin, J. Laskin and S. A. Nizkorodov, Effect of viscosity on photodegradation rates in complex secondary organic aerosol materials, *Phys. Chem. Chem. Phys.*, 2016, **18**(13), 8785–8793.

30 H. Lignell, M. L. Hinks and S. A. Nizkorodov, Exploring matrix effects on photochemistry of organic aerosols, *Proc. Natl. Acad. Sci. U. S. A.*, 2014, **111**(38), 13780–13785.

31 M. Shiraiwa, Y. Li, A. P. Tsimpidi, V. A. Karydis, T. Berkemeier, S. N. Pandis, J. Lelieveld, T. Koop and U. Poschl, Global distribution of particle phase state in atmospheric secondary organic aerosols, *Nat. Commun.*, 2017, **8**, 7.

32 D. M. Cwiertny, G. J. Hunter, J. M. Pettibone, M. M. Scherer and V. H. Grassian, Surface Chemistry and Dissolution of alpha-FeOOH Nanorods and Microrods: Environmental Implications of Size-Dependent Interactions with Oxalate, *J. Phys. Chem. C*, 2009, **113**(6), 2175–2186.

33 L. Deguillaume, M. Leriche, K. Desboeufs, G. Mailhot, C. George and N. Chaumerliac, Transition metals in atmospheric liquid phases: sources, reactivity, and sensitive parameters, *Chem. Rev.*, 2005, **105**(9), 3388–3431.

34 R. Wang, Y. Balkanski, O. Boucher, L. Bopp, A. Chappell, P. Ciais, D. Hauglustaine, J. Peñuelas and S. Tao, Sources, transport and deposition of iron in the global atmosphere, *Atmos. Chem. Phys.*, 2015, **15**(11), 6247–6270.

35 R. C. Moffet, H. Furutani, T. C. Rödel, T. R. Henn, P. O. Sprau, A. Laskin, M. Uematsu and M. K. Gilles, Iron speciation and mixing in single aerosol particles from the Asian continental outflow, *J. Geophys. Res.: Atmos.*, 2012, **117**(D7), D07204.

36 E. Journet, K. V. Desboeufs, S. Caquineau and J. L. Colin, Mineralogy as a critical factor of dust iron solubility, *Geophys. Res. Lett.*, 2008, **35**(7), 5.

37 N. M. Mahowald, S. Engelstaedter, C. Luo, A. Sealy, P. Artaxo, C. Benitez-Nelson, S. Bonnet, Y. Chen, P. Y. Chuang, D. D. Cohen, F. Dulac, B. Herut, A. M. Johansen, N. Kubilay, R. Losno, W. Maenhaut, A. Paytan, J. A. Prospero, L. M. Shank and R. L. Siefert, Atmospheric Iron Deposition: Global Distribution, Variability, and Human Perturbations, *Annu. Rev. Mar. Sci.*, 2009, **1**, 245–278.

38 Z. B. Shi, M. D. Krom, T. D. Jickells, S. Bonneville, K. S. Carslaw, N. Mihalopoulos, A. R. Baker and L. G. Benning, Impacts on iron solubility in the mineral dust by processes in the source region and the atmosphere: a review, *Aeolian Res.*, 2012, **5**, 21–42.

39 C. Weller, S. Horn and H. Herrmann, Photolysis of Fe(III) carboxylato complexes: Fe(II) quantum yields and reaction mechanisms, *J. Photochem. Photobiol., A*, 2013, **268**, 24–36.

40 H. B. Abrahamson, A. B. Rezvani and J. G. Brushmiller, Photochemical and spectroscopic studies of complexes of iron(III) with citric acid and other carboxylic acids, *Inorg. Chim. Acta*, 1994, **226**(1-2), 117–127.

41 G. R. Wentworth and H. A. Al-Abadleh, DRIFTS studies on the photosensitized transformation of gallic acid by iron(III) chloride as a model for HULIS in atmospheric aerosols, *Phys. Chem. Chem. Phys.*, 2011, **13**(14), 6507–6516.

42 T. B. Nguyen, M. M. Coggon, R. C. Flagan and J. H. Seinfeld, Reactive Uptake and Photo-Fenton Oxidation of Glycolaldehyde in Aerosol Liquid Water, *Environ. Sci. Technol.*, 2013, **47**(9), 4307–4316.

43 D. A. Thomas, M. M. Coggon, H. Lignell, K. A. Schilling, X. Zhang, R. H. Schwantes, R. C. Flagan, J. H. Seinfeld and J. L. Beauchamp, Real-Time Studies of Iron Oxalate-Mediated Oxidation of Glycolaldehyde as a Model for Photochemical Aging of Aqueous Tropospheric Aerosols, *Environ. Sci. Technol.*, 2016, **50**(22), 12241–12249.

44 S. A. Styler and D. J. Donaldson, Heterogeneous Photochemistry of Oxalic Acid on Mauritanian Sand and Icelandic Volcanic Ash, *Environ. Sci. Technol.*, 2012, **46**(16), 8756–8763.

45 A. P. Bateman, S. A. Nizkorodov, J. Laskin and A. Laskin, Time-resolved molecular characterization of limonene/ozone aerosol using high-resolution electrospray ionization mass spectrometry, *Phys. Chem. Chem. Phys.*, 2009, **11**(36), 7931–7942.

46 X. Chen, P. K. Hopke and W. P. L. Carter, Secondary Organic Aerosol from Ozonolysis of Biogenic Volatile Organic Compounds: Chamber Studies of Particle and Reactive Oxygen Species Formation, *Environ. Sci. Technol.*, 2011, **45**(1), 276–282.

47 A. E. Grigorev, I. E. Makarov and A. K. Pikaev, Formation of Cl_2^--in the bulk solution during the radiolysis of concentrated aqueous-solutions of chlorides, *High Energy Chem.*, 1987, **21**(2), 99–102.

48 R. D. Deegan, O. Bakajin, T. F. Dupont, G. Huber, S. R. Nagel and T. A. Witten, Capillary flow as the cause of ring stains from dried liquid drops, *Nature*, 1997, **389**(6653), 827–829.

49 D. E. Romonosky, N. N. Ali, M. N. Saiduddin, M. Wu, H. J. Lee, P. K. Aiona and S. A. Nizkorodov, Effective absorption cross sections and photolysis rates of anthropogenic and biogenic secondary organic aerosols, *Atmos. Environ.*, 2016, **130**, 172–179.

50 J. A. de Gouw, P. D. Goldan, C. Warneke, W. C. Kuster, J. M. Roberts, M. Marchewka, S. B. Bertman, A. A. P. Pszenny and W. C. Keene, Validation of proton transfer reaction-mass spectrometry (PTR-MS) measurements of gas-phase organic compounds in the atmosphere during the New England Air Quality Study (NEAQS) in 2002, *J. Geophys. Res.: Atmos.*, 2003, **108**(D21), 18.

51 J. de Gouw and C. Warneke, Measurements of volatile organic compounds in the earths atmosphere using proton-transfer-reaction mass spectrometry, *Mass Spectrom. Rev.*, 2007, **26**(2), 223–257.

52 M. Baasandorj, D. B. Millet, L. Hu, D. Mitroo and B. J. Williams, Measuring acetic and formic acid by proton-transfer-reaction mass spectrometry: sensitivity, humidity dependence, and quantifying interferences, *Atmos. Meas. Tech.*, 2015, **8**(3), 1303–1321.

53 L. Renbaum-Wolff, J. W. Grayson, A. P. Bateman, M. Kuwata, M. Sellier, B. J. Murray, J. E. Shilling, S. T. Martin and A. K. Bertram, Viscosity of alpha-pinene secondary organic material and implications for particle growth and reactivity, *Proc. Natl. Acad. Sci. U. S. A.*, 2013, **110**(20), 8014–8019.

54 C. Warneke, C. van der Veen, S. Luxembourg, J. A. de Gouw and A. Kok, Measurements of benzene and toluene in ambient air using proton-transfer-reaction mass spectrometry: calibration, humidity dependence, and field intercomparison, *Int. J. Mass Spectrom.*, 2001, **207**(3), 167–182.

55 A. Tani, S. Hayward, A. Hansel and C. N. Hewitt, Effect of water vapour pressure on monoterpene measurements

using proton transfer reaction-mass spectrometry (PTR-MS), *Int. J. Mass Spectrom.*, 2004, **239**(2-3), 161–169.

56 A. Vlasenko, A. M. Macdonald, S. J. Sjostedt and J. P. D. Abbatt, Formaldehyde measurements by Proton transfer reaction – Mass Spectrometry (PTR-MS): correction for humidity effects. Atmospheric, *Meas. Tech.*, 2010, **3**(4), 1055–1062.

57 A. Virkkula, R. Van Dingenen, F. Raes and J. Hjorth, Hygroscopic properties of aerosol formed by oxidation of limonene, alpha-pinene, and beta-pinene, *J. Geophys. Res.: Atmos.*, 1999, **104**(D3), 3569–3579.

58 R. Battino, T. R. Rettich and T. Tominaga, The Solubility of Oxygen and Ozone in Liquids, *J. Phys. Chem. Ref. Data*, 1983, **12**(2), 163–178.

59 E. Kostenidou, R. K. Pathak and S. N. Pandis, An algorithm for the calculation of secondary organic aerosol density combining AMS and SMPS data, *Aerosol Sci. Technol.*, 2007, **41**(11), 1002–1010.

60 D. M. Lienhard, A. J. Huisman, U. K. Krieger, Y. Rudich, C. Marcolli, B. P. Luo, D. L. Bones, J. P. Reid, A. T. Lambe, M. R. Canagaratna, P. Davidovits, T. B. Onasch, D. R. Worsnop, S. S. Steimer, T. Koop and T. Peter, Viscous organic aerosol particles in the upper troposphere: diffusivity-controlled water uptake and ice nucleation?, *Atmos. Chem. Phys.*, 2015, **15**(23), 13599–13613.

61 H. C. Price, B. J. Murray, J. Mattsson, D. O'Sullivan, T. W. Wilson, K. J. Baustian and L. G. Benning, Quantifying water diffusion in high-viscosity and glassy aqueous solutions using a Raman isotope tracer method, *Atmos. Chem. Phys.*, 2014, **14**(8), 3817–3830.

62 H. C. Price, J. Mattsson, Y. Zhang, A. K. Bertram, J. F. Davies, J. W. Grayson, S. T. Martin, D. O'Sullivan, J. P. Reid, A. M. J. Rickards and B. J. Murray, Water diffusion in atmospherically relevant alpha-pinene secondary organic material, *Chem. Sci.*, 2015, **6**(8), 4876–4883.

63 Y. Chenyakin, D. A. Ullmann, E. Evoy, L. Renbaum-Wolff, S. Kamal and A. K. Bertram, Diffusion coefficients of organic molecules in sucrose-water solutions and comparison with Stokes-Einstein predictions, *Atmos. Chem. Phys.*, 2017, **17**(3), 2423–2435.

64 R. F. Hems, J. S. Hsieh, M. A. Slodki, S. Zhou and J. P. D. Abbatt, Suppression of OH Generation from the Photo-Fenton Reaction in the Presence of α-Pinene Secondary Organic Aerosol Material, *Environ. Sci. Technol. Lett.*, 2017, **4**(10), 439–443.